

Computational advantage from quantum superposition of multiple temporal orders of photonic gates

Márcio M. Taddei,^{1,2,*} Jaime Cariñe,^{3,4,5} Daniel Martínez,^{3,4} Tania García,^{3,4} Nayda Guerrero,^{3,4} Alastair A. Abbott,^{6,7} Mateus Araújo,⁸ Cyril Branciard,⁹ Esteban S. Gómez,³ Stephen P. Walborn,^{3,4} Leandro Aolita,^{1,10} and Gustavo Lima^{3,4}

¹*Instituto de Física, Federal University of Rio de Janeiro, 21941-972, P. O. Box 68528, Rio de Janeiro, Brazil*

²*ICFO - Institut de Ciències Fotòniques, The Barcelona Institute of Science and Technology, 08860, Castelldefels, Barcelona, Spain*

³*Departamento de Física, Universidad de Concepción, 160-C Concepción, Chile*

⁴*ANID – Millennium Science Initiative Program – Millennium Institute for Research in Optics, Universidad de Concepción, 160-C Concepción, Chile*

⁵*Departamento de Ingeniería Eléctrica, Universidad Católica de la Santísima Concepción, Alonso de Ribera 2850, Concepción, Chile*

⁶*Department of Applied Physics, University of Geneva, 1211 Geneva, Switzerland*

⁷*Univ. Grenoble Alpes, Inria, 38000 Grenoble, France*

⁸*Institute for Quantum Optics and Quantum Information (IQOQI),*

Austrian Academy of Sciences, Boltzmannngasse 3, 1090 Vienna, Austria

⁹*Univ. Grenoble Alpes, CNRS, Grenoble INP, Institut Néel, 38000 Grenoble, France*

¹⁰*Quantum Research Centre, Technology Innovation Institute, Abu Dhabi, UAE*

Models for quantum computation with circuit connections subject to the quantum superposition principle have been recently proposed. There, a control quantum system can coherently determine the order in which a target quantum system undergoes N gate operations. This process, known as the quantum N -switch, is a resource for several information-processing tasks. In particular, it provides a computational advantage — over fixed-gate-order quantum circuits — for phase-estimation problems involving N unknown unitary gates. However, the corresponding algorithm requires an experimentally unfeasible target-system dimension (super-)exponential in N . Here, we introduce a promise problem for which the quantum N -switch gives an equivalent computational speed-up with target-system dimension as small as 2 regardless of N . We use state-of-the-art multi-core optical-fiber technology to experimentally demonstrate the quantum N -switch with $N=4$ gates acting on a photonic-polarization qubit. This is the first observation of a quantum superposition of more than $N=2$ temporal orders, demonstrating its usefulness for efficient phase-estimation.

I. INTRODUCTION

Quantum mechanics allows for processes where two or more events take place in a quantum superposition of different temporal orders. This exotic phenomenon results in causal nonseparability [1–3], and it is likely to be especially relevant in quantum treatments of gravity [4–6]. In fact, quantum control of temporal orders could be realized with quantum circuits exploiting hypothetical closed time-like curves [7, 8], and it would also arise naturally due to the spacetime warping that macroscopic spatial superpositions of massive bodies would cause [9].

From a more practical perspective, advanced quantum computational models without definite gate orders have sparked a great deal of fundamental interest, as they do not fit into the usual paradigm of circuits with fixed gate connections [6, 7, 10–13]. The best known example is the celebrated quantum N -switch gate, S_N , which coherently applies a different permutation of N given gates on a target quantum system conditioned on the state of a control quantum system [7, 13, 14]. S_N has been identified as a resource for a number of exciting information-theoretic tasks. For instance, for $N=2$, it allows one to deterministically distinguish pairs of commuting versus anti-commuting unitaries [12]; and, remarkably, this translates into an exponential advantage in a communication complexity problem [15, 16].

In general, circuits that synthesize S_N with a fixed gate order are known, but at the expense of quadratically more queries to (i.e., uses of) the gates [12–14, 17]. As a consequence thereof, S_N allows one to solve a promise problem [12, 14] on the permutations of N unknown unitary gates with quadratically fewer queries in N than all known circuits with fixed gate order. More precisely, the permutation sequences of the gates are promised to differ only by a phase factor, and S_N efficiently estimates these phase differences. However, the algorithm for this problem [12, 14] requires the target-system dimension to grow (super-)exponentially with N , making it experimentally demanding. As a matter of fact, all experimental realizations of the quantum N -switch reported so far are restricted to the simplest case of $N=2$ gate orders [16, 18–22].

In this work, we introduce a novel algorithm that exploits the quantum N -switch and experimentally demonstrate it for $N=4$ unitary gates. Specifically, we find a variant of the above phase-estimation problem, which we name the Hadamard promise problem, for which the quantum N -switch is also a resource but with considerably milder constraints on the target-system dimension. On one hand, this problem plays a role in computation with indefinite gate orders analogous to Deutsch-Jozsa’s [23] or Simon’s [24] problems in the beginnings of quantum computation: a proof-of-principle of improvements over a previous paradigm. On the other hand, there are reasons to expect that practical applications of the Hadamard promise problem will be developed, both because closely related phase-estimation problems already have many

* marciotaddei [at] gmail.com

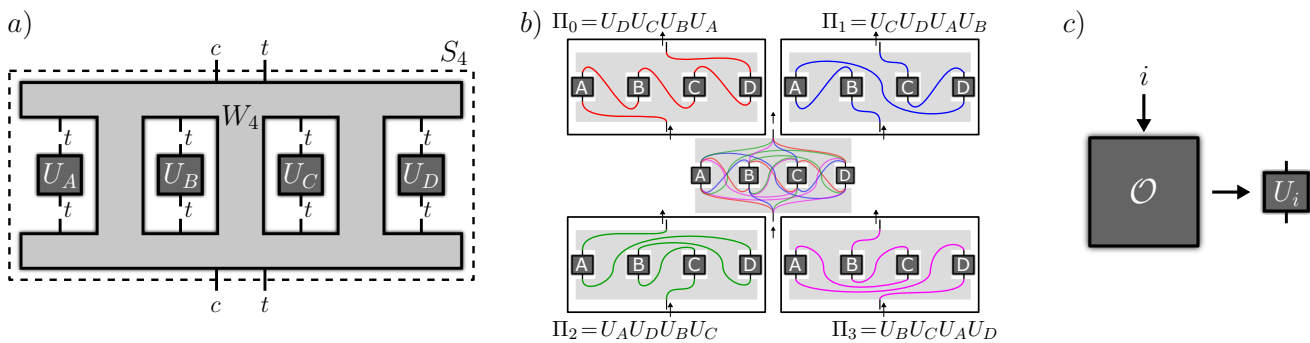


Figure 1. *a)* Abstract representation of the quantum N -switch for the case of $N = 4$. The process, W_4 (light-grey region), can be thought of as an experimental setup (e.g., a quantum circuit or interferometer) through which the composite control-target system goes and with open slots for target-subsystem gates U_i (dark-grey boxes), for $i = A, B, C$, or D , to be inserted. Inside W_4 , the connections between these gates are coherently controlled by the control subsystem, an effect known as quantum control of gate orders (QCGO). This property is a physical resource for certain quantum computations (phase-estimation problems), and W_4 is the resourceful object that bears it. The concatenation of W_4 with the inserted gates yields the quantum 4-switch gate S_4 , a joint unitary operation on the composite system. *b)* Concrete schematics of the specific variant of the quantum 4-switch process experimentally implemented in this work. The target subsystem undergoes the four-gate sequence in a quantum superposition (center) of $P = 4$ different orderings (permutations of the string $ABCD$): $ABCD, BADC, CBDA, DACB$. Each permutation is shown individually in a different color and panel. *c)* In the above-mentioned computations, the target-subsystem gates are unknown. For the purpose of complexity analysis, they can be thought of as produced upon request by a quantum oracle \mathcal{O} . This takes as input $i = A, B, C$, or D and outputs a black-box device implementing the unknown gate U_i . Each such call to the oracle counts as an oracle query. The N -switch process allows one to solve computational problems on the phase relationships between permutations of the black-box gates with considerably fewer oracle queries – i.e. lower query complexity – than any process with fixed (or classically controlled) gate connections.

applications, and because it involves the quantum Fourier transform, which is an important sub-routine for a variety of quantum algorithms with practical applications [25]. The problem’s promise is that the products of the N unknown gates applied in P different orders differ only in $+$ or $-$ signs that are encoded into one of the columns of a given $P \times P$ -dimensional Hadamard matrix; and the problem consists of finding which column it is.

The algorithm to solve this problem exploits the quantum N -switch – consuming N queries to the gates – to deterministically find the column. This represents a speed-up quadratic in N in query complexity (i.e. number of queries) with respect to all known algorithms exploiting circuits with fixed gate orders (see [14, 26, 27] for a discussion of how to count queries in a quantum switch). Hence, the algorithm is not only an interesting computational primitive on its own but also a practical tool to benchmark experimental realizations of S_N , because the quantum N -switch is the only known process for which the algorithm succeeds with unit probability for all gates satisfying the promise while only consuming N gate queries. To demonstrate the practicability of the algorithm we implement it with a quantum N -switch of $N = 4$ gates using modern multi-core optical-fiber technology [28–31]. The 4 gates are implemented on the target polarization qubits using programmable liquid-crystal devices, and the spatial degree of freedom of a single photon is used as the control system. We obtain an average success probability for the algorithm, over different sets of gates, of $p_{\text{succ}} \approx 0.95$. Our results represent the first demonstration of the quantum N -switch gate for N larger than 2, as well as of its efficiency for phase estimation problems involving multiple unknown gates.

II. PRELIMINARIES

Quantum control of gate orders

In quantum computation, a quantum switch can be described by a special type of controlled operation that applies a particular unitary gate Π_x to a target system (t) for each different state of a control system (c). We define the quantum N -switch gate as

$$S_N |x\rangle_c |\Psi\rangle_t = |x\rangle_c \Pi_x |\Psi\rangle_t, \quad (1)$$

where $|x\rangle_c$ is the x -th member of the computational basis of the control system, and $|\Psi\rangle_t$ is an arbitrary state of the target system. The heart of the quantum N -switch is the operator $\Pi_x := U_{\sigma_x(N-1)} \dots U_{\sigma_x(1)} U_{\sigma_x(0)}$, which is a product of the N unitary gates in a fixed set $\mathcal{U} := \{U_A, U_B, \dots\}$, in their x -th ordering. More precisely, σ_x is a vector with N elements specifying the x -th permutation of the N gates in \mathcal{U} , i.e. it specifies the ordering sequence of the unitaries, so that $\sigma_x(j)$ is the j -th element in the x -th permutation. To control the implementation of P different permutations of gates requires a control system of at least dimension P . The dimension of the target system can be arbitrary and we denote it as d . With S_N defined as in (1), it is clear that c coherently controls the order of the N unitary gates applied to system t , which explains the name “quantum control of gate orders” (QCGO). We note that the usual definition [13, 14] of the quantum N -switch deals only with the specific case of all $N!$ permutations of the gates in \mathcal{U} . However, here (as in Refs.[32, 33]) we will be interested in the more general case $P \leq N!$.

Clearly, the general definition of QCGO is independent of the specific choice of gates in \mathcal{U} . A convenient mathemati-

cal tool to capture that is the quantum N -switch process W_N , which produces the quantum N -switch gate S_N when given the set of gates U as input. For the technical definition of processes, we refer the reader to Refs. [1–3, 34]. Intuitively, one can think of a process as the quantum evolution generated by an experimental arrangement with open slots for gates on the target system to be inserted [10, 11], as represented in Fig. 1 (a). Inside the process, the connections between the inserted gates may be subject to the quantum superposition principle. For instance, Fig. 1 (b) pictorially represents our experimental implementation of the quantum 4-switch S_4 , with a coherent quantum superposition of $P = 4$ different gate connections (each one in a different color), for the particular choice of permutation set $\{ABCD, BADC, CBDA, DACB\}$. Such superpositions give rise to QCGO, which corresponds to a specific type of quantum control of causal orders[35] (and both phenomena are in turn contained within the general notion of causal nonseparability [1–3]). In particular, QCGO takes place when those gate connections are coherently controlled by a control system, as in Eq. (1). Aside from being a fundamentally interesting phenomenon, QCGO turns out to be a physical resource for interesting phase-estimation problems, as we discuss next.

The Araújo-Costa-Brukner algorithm

The quantum N -switch process provides an advantage for solving a particular phase-estimation problem [12, 14] to which we here refer as the Fourier promise problem. In this type of problems, one has access to a quantum oracle \mathcal{O} for U , i.e. a black-box device that delivers a gate $U_i \in U$ every time it is queried. See Fig. 1 (c). No information about the gates is available except for the promise that, for the constant phase factor $\omega := e^{i\frac{2\pi}{P}}$ and for all $x \in [P]$, they satisfy the property:

$$\Pi_x = \omega^{xy} \Pi_0, \quad (2)$$

for some fixed, unknown $y \in [P]$, where the short-hand notation $[P] := \{0, 1, \dots, P-1\}$ has been introduced. The task is to determine which one of the properties holds, i.e. to find y .

The Araújo-Costa-Brukner algorithm to solve this problem is based on the standard Hadamard test [36], and shares similarities with the Kitaev phase estimation algorithm [37]. The control system is initialized in the computational-basis reference state $|0\rangle_c$, while the target system starts in an arbitrary state $|\Psi\rangle_t$. A P -dimensional quantum Fourier transform F_P on c maps it to a uniform superposition of all computational-basis states. Then, the quantum N -switch gate is applied. Because of property (2), this introduces the phase factor ω^{xy} to each computational-basis state $|x\rangle_c$ in the superposition, while the state $\Pi_0 |\Psi\rangle_t$ of the target system factorizes. The value of y is thus encoded into the phases of the superposition state of the control system. To map it back to the computational basis, one uncomputes the Fourier transform (applying its inverse $F_P^{-1} = F_P^\dagger$). In symbols [14]:

$$F_P^{-1} S_N F_P |0\rangle_c |\Psi\rangle_t = |y\rangle_c \Pi_0 |\Psi\rangle_t. \quad (3)$$

Then, y is finally read out by a single-shot computational-basis measurement on c .

To apply S_N , one must consume N queries to \mathcal{O} . Therefore, the query complexity – i.e. total number of oracle queries – of the algorithm is $Q = N$, for all $P \leq N!$. Remarkably, causally ordered processes (i.e., those produced by circuits with fixed, or classically controlled, gate connections) require considerably more queries to solve the same problem. For instance, for $P = N!$, the best causally ordered process displays query complexity $Q = \Omega(N^2)$ [13, 14, 17], i.e. quadratically higher in N . A downside of the algorithm, however, is that the target-system dimension d must grow with the number P of gate orders. This can be seen[14] by taking the determinant of both sides of Eq. (2). For $y = 1$, and since $\det \Pi_x = \det \Pi_0$, this imposes $\det \Pi_0 = \omega^{xd} \det \Pi_0$ (and, hence, $1 = e^{i\frac{2\pi}{P}xd}$), for all $x \in [P]$, which is possible only if $d \geq P$. This constraint is especially significant for experimental realizations, where coherently manipulating high-dimensional target systems together with high-dimensional control systems is challenging [16]. For example, this limitation implies that if the polarization of a single photon ($d = 2$) is used as the target system, the algorithm is useful only for $P = 2$; despite the fact that the spatial degree of freedom of the photon is amenable to encode much higher-dimensional control systems [38]. To overcome this, we next introduce another variant of phase-estimation problem that is considerably less sensitive to the determinant constraint.

III. A NEW COMPUTATIONAL PRIMITIVE: THE HADAMARD PROMISE PROBLEM

We consider a different promise on the gates that the oracle \mathcal{O} outputs. Given a known $P \times P$ -dimensional square matrix M_P of entries $m_{x,y} = \pm 1$, we require that the black-box unitaries in U satisfy, for all $x \in [P]$, the property:

$$\Pi_x = m_{x,y} \Pi_0, \quad (4)$$

for some fixed, *a priori* unknown matrix column $y \in [P]$. The task is, again, to find out y . In contrast to the complex-phase relation of Eq. (2), the constraint that this real-phase relation imposes on d is much softer. As one can see taking the determinant of both sides of Eq. (4), the only requirement that arises now is that $(m_{x,y})^d = 1$ for all $x, y \in [P]$, which is satisfied by any even d . With this, the promise problem finds application even when the target system is a simple qubit, regardless of the number of permutations P . Instead of a single complex phase factor, the value of y is now encoded in a string of P real phase factors (i.e., a column of M_P). The question, then, is how to decode that information. Luckily, the value of y can be mapped back onto the computational basis of c with a simple procedure, similar to that in Eq. (3), provided that M_P is a *Hadamard matrix* [36].

A Hadamard matrix (of order P) is a $P \times P$ -dimensional square matrix M_P with entries $m_{x,y} = \pm 1$ and whose columns (or equivalently, whose rows) are all mutually orthogonal. The transpose M_P^T of M_P is proportional to its inverse: $\frac{1}{P} M_P \cdot M_P^T = \mathbb{1}$, with $\mathbb{1}$ the identity matrix. Such

matrices can only exist for P equal to 1, 2 or integer multiples of 4, and are conjectured to exist for all such dimensions. In fact, they can be generated recursively for any $P = 2^k$, with $k \in \mathbb{N}$. Here we are actually interested in the subset of Hadamard matrices with all +1's in the first row ($x = 0$) and column ($y = 0$). The former condition is required by Eq. (4), whereas the latter condition is necessary in our algorithm below for correct encoding (see App. 1 for details). With this, we can formally rephrase this promise problem as follows.

Problem 1 (Hadamard promise problem). *Given a Hadamard matrix M_P with all +1 entries along its first row and column and a unitary-gate oracle \mathcal{O} fulfilling the promise – i.e. Eq. (4) for some column $y \in [P]$ of M_P –, compute y .*

The algorithm to solve it with the quantum N -switch gate is similar to the Araújo-Costa-Brukner algorithm but with the quantum Hadamard gate H_P associated to M_P playing the role of F_P . The matrix representation of H_P in the computational basis is $H_P := \frac{M_P}{\sqrt{P}}$. Then, the following algorithm solves Problem 1.

Algorithm 1. *Initialize the joint system in the state $|0\rangle_c |\Psi\rangle_t$, with $|\Psi\rangle_t$ an arbitrary target state. Then, apply H_P on c . Then, apply S_N on the joint control-target system. Then, apply H_P^{-1} ($= H_P^\dagger$) on c . This gives the state*

$$H_P^{-1} S_N H_P |0\rangle_c |\Psi\rangle_t = |y\rangle_c \Pi_0 |\Psi\rangle_t. \quad (5)$$

Finally, read out y as the outcome of a single-shot computational-basis measurement on c .

This algorithm thus provides the desired phase relation between the P different permutations of the N unknown unitaries under consideration. The validity of Eq. (5) is proven explicitly in App. 1. The query complexity of the algorithm is the same as that of the Araújo-Costa-Brukner algorithm: $Q = N$ for all $P \leq N!$. The crucial resource for Algorithm 1 is the quantum N -switch process. Similarly to the Fourier promise problem [14], no causally ordered process is known to solve Problem 1 in general (i.e., for any arbitrary set U of unknown gates fulfilling the promise) with a query complexity linear in N . In fact, the (query-wise) optimal causally ordered processes known to solve the problem in general are simply the fixed-gate circuits that simulate the quantum N -switch exactly (see Methods section), but these require considerably more queries [13, 14, 17]. For instance, in the case where all gate permutations are considered ($P = N!$), simulating the quantum N -switch exactly in the blackbox scenario requires $Q = \Omega(N^2)$ oracle queries, i.e. quadratically higher in N . Another concrete example is the quantum 4-switch process for the $P = 4$ permutations in the set $\{ABCD, BADC, CBDA, DACB\}$ [shown in Fig. 1 (b)], whose experimental implementation we describe below. The optimal circuit to simulate it exactly in the blackbox scenario requires $Q = 9$ oracle queries, i.e. more than twice as many as with S_4 (see App. 2).

Table 1a					Table 1b				
y	0	1	2	3	y	0	1	2	3
U_A	$\mathbb{1}$	Z	$\mathbb{1}$	Z	U_A	$\frac{Z+X}{\sqrt{2}}$	$\mathbb{1}$	Z	Z
U_B	X	X	X	X	U_B	$\frac{Z+X}{\sqrt{2}}$	X	X	X
U_C	$\mathbb{1}$	Z	Z	$\mathbb{1}$	U_C	$\mathbb{1}$	Z	$\mathbb{1}$	$\mathbb{1}$
U_D	X	X	X	X	U_D	$\mathbb{1}$	$\mathbb{1}$	$\mathbb{1}$	X

Table 1. Tables of polarization unitaries used for the implementations of two different quantum 4-switch gates (both with the same set of gate permutations $\{ABCD, BADC, CBDA, DACB\}$; here $\mathbb{1}$ is the identity, Z and X are the Pauli operators). For both tables, each column provides a different set U of oracle gates. In turn, each such set exhibits the phase relations encoded – via Eq. (4) – in the corresponding column y of the matrix in Eq. (6). That is, the implemented oracle gates fulfill the problem's promise with respect to the experimentally-implemented Hadamard matrix and the chosen set of permutations.

IV. EXPERIMENTAL QUANTUM CONTROL OF THE ORDER OF MULTIPLE GATE OPERATIONS

The experiment is illustrated in Fig. 2 (a). It is based on multi-core optical fibers and new related technology [28], which was recently introduced as a toolbox for quantum information processing [29–31]. In our implementation of the quantum 4-switch, the control system corresponds to the spatial mode of a single photon, while the target is its polarization. Following Algorithm 1, a conventional illumination scheme (see Methods) is used to generate single photons propagating over a single-mode fiber in the initial spatial mode state $|0\rangle_c$. The photons are then sent through a four-core fiber beam splitter (4CF-BS), which has been shown to realize with high-fidelity the $H_4 = \frac{M_4}{2}$ Hadamard operation given by [39]

$$H_4 = \frac{1}{2} \begin{bmatrix} 1 & 1 & 1 & 1 \\ 1 & 1 & -1 & -1 \\ 1 & -1 & -1 & 1 \\ 1 & -1 & 1 & -1 \end{bmatrix}. \quad (6)$$

Note that this matrix is self-inverse. The 4CF-BS is placed between commercial spatial multiplexer/demultiplexer (DMUX) units [40, 41], which couple four single-mode fibers (yellow fibers) to the four cores of the multi-core fibers (green fibers). These units connect to the 4CF-BS through the multi-core fibers [see details in Fig. 2 (b)].

After transmission through the 4CF-BS, the photon is sent to the quantum 4-switch gate S_4 , which will coherently apply different permutations of four unitary operations U_i on the target system (photon polarization), depending on the spatial mode. To see this, note that each output of the 4CF-BS routes the photon through a different ordering of the polarization operations U_i , which are realized with controllable liquid crystal retarders (LCR). To control the implementation order of the U_i 's, we take advantage of the DMUX units. Each single-mode fiber input to the quantum 4-switch gate is connected to a different four-core fiber on the IN side of S_4 using a DMUX unit. The other end of each 4CF is attached to a fiber launcher.

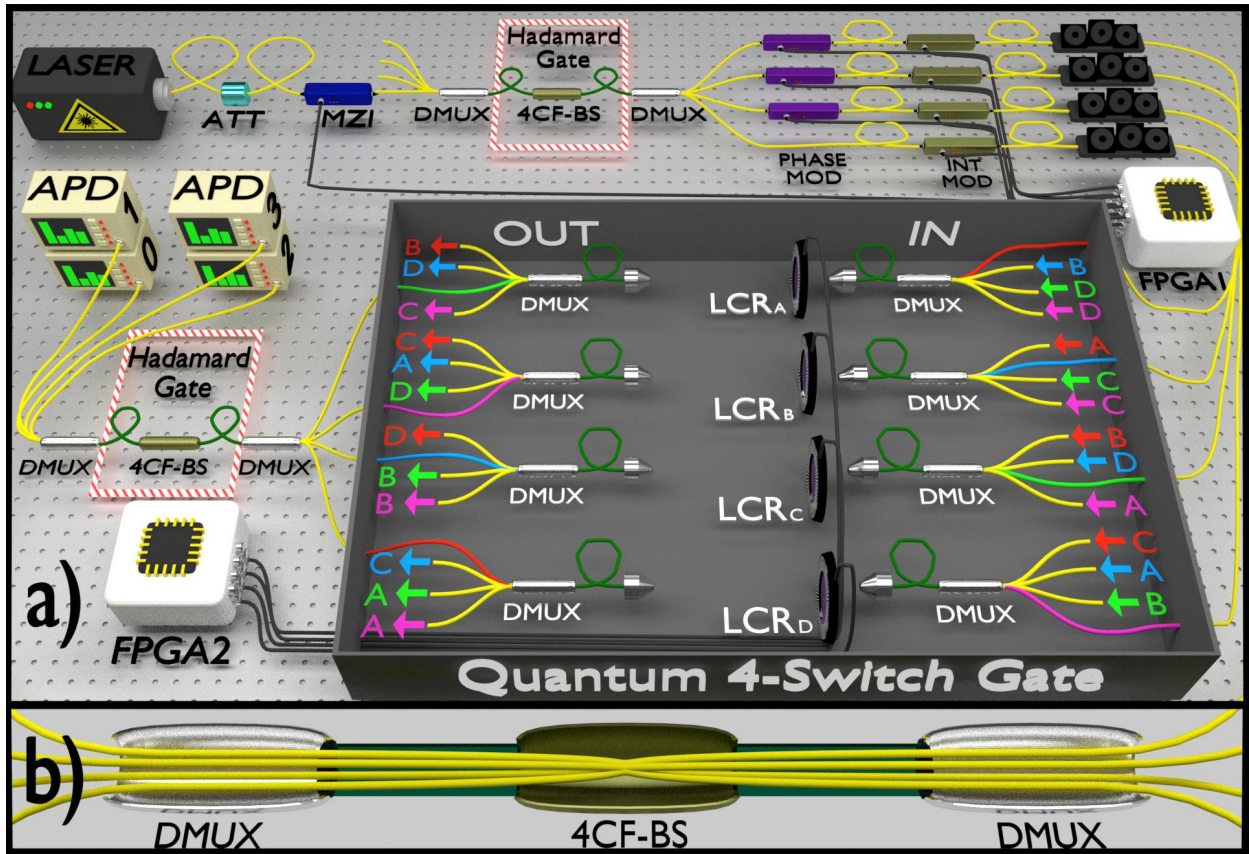


Figure 2. a) Illustration of our implementation of the quantum 4-switch gate (S_4). An input photon is divided coherently between four spatial modes using a four-core fiber beam splitter (4CF-BS), placed between commercial multiplexer/demultiplexer (DMUX) units, as shown in b). The four output modes are then sent to the quantum 4-switch S_4 . Each spatial mode is related to a unique permutation of the four unitary polarization operations applied by S_4 and indicated by a different color. The photons enter through the IN side (right) and exit through the OUT side (left), where, for example, the notation “ $\leftarrow A$ ” means “from A” and “ $A \leftarrow$ ” means “to A”. One can follow a certain path by looking at the output labels. For instance, the green input mode enters in C and continues to “ B , then D , then A , and finally exit”, corresponding to the operation of the four polarization unitaries in the order $CBDA$. After S_4 , the four spatial modes are then recombined using a second 4CF-BS. Each output 0–3 is connected directly to a single-photon detector (APD). The detection of a single-photon in the y -th ($y = 0, 1, 2, 3$) output detector identifies in a single-shot the phase relation y of the four unitaries implemented in the quantum 4-switch gate. See the main text and Methods for further details.

The photon leaves the launcher in free space passing through the LCR and is coupled back into another 4CF on the OUT side. The OUT 4CF is connected (via another DMUX) to single mode fibers, which are then connected to the next 4CF (exploiting the already installed DMUXs) back on the 4-switch’s IN side, following the ordering showed in Fig. 2 (a). For example, a photon in the green input undergoes the operation of the four unitaries in the order $C \rightarrow B \rightarrow D \rightarrow A$, resulting in the product unitary $\Pi_2 = U_A U_D U_B U_C$. The other three inputs lead the photon through one of the other three permutations shown in the insets of Fig. 1 (b). After S_4 , a second Hadamard operation is applied to the control system using a second set of DMUX/4CF-BS/DMUX, in accordance with Algorithm 1. The setup is thus a four-arm interferometer with each output directly connected to an InGaAs single-photon detector (APD), working in gated mode and configured with 10% overall detection efficiency, and 5 ns gate width. The detection of a single-photon in the y -th ($y = 0, 1, 2, 3$) out-

put detector univocally identifies in a single-shot the property y indicating the phase relations of the four unitaries implemented in the quantum 4-switch gate.

Before implementing the quantum 4-switch, an initial alignment procedure using a polarimeter is performed. In-fiber polarization controllers (not shown in Fig. 2) are used in all single-mode fibers of the quantum 4-switch to ensure that every fiber corresponds to an identity operation on the polarization. They are also used at the final set of DMUX/4CF-BS/DMUX to guarantee the indistinguishability of the core modes, such that there is no path-information available that would compromise the visibility of the interferometer [42, 43]. The LCRs implementing the unitaries can be adjusted between identity and a half-wave plate by controlling the input voltage. In this way, we can toggle between an identity operation $\mathbb{1}$ and one of the Pauli operators Z , $(Z + X)/\sqrt{2}$ or X , when the orientation angle of the LCR is 0° , 22.5° or 45° , respectively. Importantly, we note that the

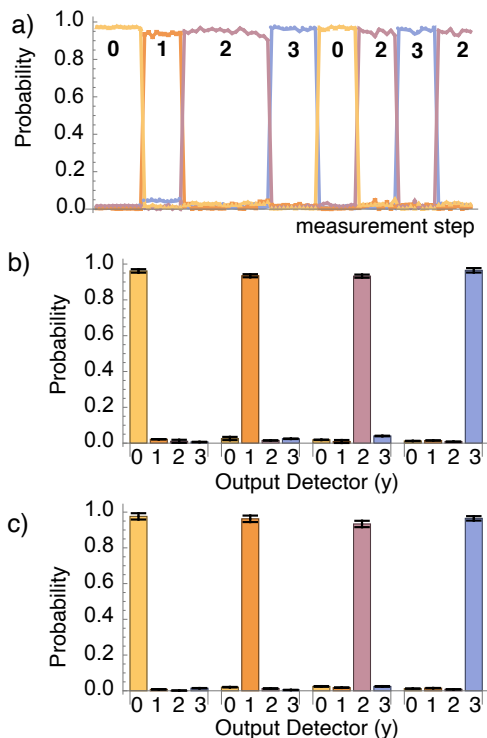


Figure 3. a) A sequence of about 8 min of measurement results with our quantum 4-switch process taken in real time. Measurements of 0.1s duration were taken continuously, realized within the phase stabilization routine (see Methods), in which the four sets of unitaries given each by the y -th column of Table 1a were toggled randomly every minute. The number labels correspond to the columns of Table 1a. Summary of experimentally obtained success probabilities to identify the commutation relations of the unitary operations in Table 1a [panel b)] and Table 1b [panel c)]. See text for more details.

LCRs were placed at the far-field plane of the 4CF launchers and that this guarantees that the unitary operations U_i are indistinguishable when applied in different orders (see Methods). A computer-controlled field programmable gate array (FPGA2) unit is used to control the LCRs.

In Table 1 we list the polarization operations U_i for two different implementations of the quantum 4-switch. Table 1a corresponds to orthogonal operations (for each given column), while Table 1b includes non-orthogonal ones, which makes it more difficult to mimic the quantum N -switch with a causally ordered process (see below and App. 3). In each table, the y -th column defines a different set U of the target-system unitary gates and corresponds to the y -th column of the Hadamard matrix in Eq. (6) (see Methods). In our experiment, by exploiting the controlled LCRs, we are able to toggle between the different sets U of unitaries in real time. Fig. 3 (a) shows an example of the results recorded while switching randomly (with uniform probabilities) between operations corresponding to different columns of Table 1a, about every minute. In each 0.1 s measurement we detected a total of ~ 6000 events. Figs. 3 (b) and (c) show a summary of experimentally obtained success probabilities (each obtained from $\sim 3 \times 10^4$ events) to identify the relative-phase relations

between the different permutations of the unitary operations in Table 1a and Table 1b, resp. For Table 1a we obtain an average success probability of $p_{\text{succ}} = 0.948 \pm 0.005$, whereas for Table 1b we obtain $p_{\text{succ}} = 0.959 \pm 0.008$. Error bars correspond to one standard deviation, and are obtained by error propagation of the Poissonian count statistics. These results demonstrate the successful implementation of the quantum 4-switch process.

V. BENCHMARKING EXPERIMENTAL QUANTUM CONTROL OF MULTIPLE GATE ORDERS

To benchmark the realization of QCGO, it is useful to imagine a verification scenario, in which a Verifier controls the oracle, while the process is implemented by a Prover. The Prover wishes to prove to the Verifier that the process does display QCGO, and the Verifier can test this by asking the Prover to compute properties of oracles involving different gates. The quantum N -switch process allows the Prover to solve the computations with considerably fewer oracle queries than any process with fixed (or classically controlled) gate connections. Indeed, it is the only process known to provide a unit success probability for Problem 1 in general (i.e. for any set of black-box gates satisfying the promise) with only N queries to the oracle. This can be used to give the Verifier evidence in favour of the Prover's honesty. However, if the table of oracle-gates has a small number of columns – e.g., as in Table 1 – a dishonest Prover with side information about the table can attain $p_{\text{succ}} = 1$ with a causally ordered process (see App. 3), thus deceiving the Verifier.

One way to benchmark experimental quantum switches with minimal assumptions is by measuring so-called causal witnesses [2, 44]. Interestingly, by increasing the number of columns in the oracle-gate table (i.e., of possible choices for the gate sets U) and suitably choosing their prior probability distribution, Algorithm 1 can be turned into a causal witness for the quantum switch. That is, for sufficiently large oracle-gate tables and an appropriate prior distribution the gate sets U , an upper bound $p_{\text{succ}}^{\text{CCGO}}$ strictly smaller than one can be found for the probability of success attainable by processes with *classical* control of gate orders. This provides us with a gap from the the probability of success obtained by the quantum switch, which always remains unity in the noiseless case. Details on our search for witnesses are given in App. 4.

Unfortunately, the number of measurement settings required to measure such witnesses is prohibitively high in practice for this experimental setup. For instance, the best witness for W_4 we could obtain with the above-mentioned approach gives $p_{\text{succ}}^{\text{CCGO}} \approx 0.89$, but requires an oracle-gate table with 300 columns. Alternatively, weaker witnesses with $p_{\text{succ}}^{\text{CCGO}} \approx 0.92$ can also be found, but these still require 60 columns. Our LCR-based setup cannot switch among so many gates in a practical way. Nevertheless, it is yet a remarkable feature of our experiment that we do reach values of p_{succ} significantly higher than both bounds, which would conclusively benchmark W_4 for higher number of settings. In addition, we note that witnesses with similarly high numbers of settings (259)

have indeed been measured in other platforms, though with much slower switching times [19].

Alternatively, smaller oracle-gate tables suffice if the Verifier can actively reduce the Prover’s potential knowledge about the tables. One way to do this is by allowing the Verifier to apply a random basis rotation to each gate before delivering it to the Prover. For instance, in this scenario, an upper bound $p_{\text{succ}}^{\text{CCGO}} \approx 0.84$ can be obtained for an oracle-gate table with only 30 columns (see App. 4). Unfortunately, implementing such a causal witness would require the ability to switch among a continuum of gates, which is again experimentally infeasible. Nevertheless, here we are mainly interested in benchmarking our implementation of W_4 against experimental imperfections, rather than against hypothetical malicious Provers exploiting side-information about the gates’ bases. In this regard, the experimentally obtained values in Fig. 3 are in the range $p_{\text{succ}} \approx 0.93\text{-}0.97$, which suggests that our setup should be capable of obtaining average success probabilities that are larger than the thresholds mentioned above, for a larger number of settings. Though not yet conclusive, this provides encouraging evidence for the QCGO of the implemented process.

VI. DISCUSSION

Here we introduced the “Hadamard promise problem”, a novel computational primitive involving the relative phases between different permutations of multiple unknown gates. We presented an algorithm to solve it efficiently, illustrating a quantum computational advantage associated to the coherent quantum control of the order in which a sequence of N unitary operations is applied. Our algorithm, which we implemented experimentally for $N = 4$, exploits the quantum N -switch process to solve the problem with N applications of the unitary gates, whereas the known methods exploiting fixed gate orders use the gates $O(N^2)$ times. Both problem and algorithm have the advantage that the target system needs only be two-dimensional, as opposed to $N!$ -dimensional as in previous proposals. This could inspire new approaches for exploiting indefinite causal order in quantum computation and communication, as well as for studying causal non-separability in physical systems.

We experimentally implemented the algorithm by constructing a quantum 4-switch process that coherently controls four different gate orderings with high fidelity, showing success probabilities for the algorithm of ~ 0.95 . The all-optical setup involves a four-path interferometer constructed with new multi-core optical fiber technology. As discussed in the Methods, the best known quantum circuit with fixed gate orders solves this problem with 9 gate queries. Our experiment thus corresponds to a 5-query improvement. Moreover, this is, to the best of our knowledge, the first report of a quantum superposition of more than 2 temporal orders. In addition, our implementation presents some technical advantages as well: On the one hand, it is versatile in that the gate orders can be modified in a practical fashion by switching the optical fiber connections and that the unitary gates themselves can

be automatically controlled through the liquid crystal polarization retarders. On the other hand, the setup can be scaled up to higher control-system dimensions in a straightforward fashion. This work constitutes a key step towards realizing and verifying causal non-separability among a large number of parties, and should play an important role in developing methods to exploit this resource.

METHODS

A. Query complexity analysis

One may argue that implementing S_N is not the only way to solve Problem 1 (which is also true for the Fourier promise problem [14]). Here, we estimate the query complexity of other plausible approaches.

A natural approach one may attempt is to tomographically reconstruct the N unitary gates and then multiply them to estimate the Π_x ’s, from which one can infer y . Since each Π_x is an N -fold product of the U_i ’s, the overall error ε in its estimation is $\varepsilon = \Omega(N \epsilon)$, where ϵ is the statistical error of the reconstruction of each U_i . To attain a constant overall error one thus needs $\epsilon = O(1/N)$, which, by virtue of Hoeffding’s bound, in turn requires $q = O(1/\epsilon^2) = O(N^2)$ queries to each U_i . Moreover, since there are N gates to reconstruct, the overall query complexity is $Q = O(Nq) = O(N^3)$, i.e. cubically worse in N than with the quantum N -switch. Another alternative is to tomographically reconstruct each Π_x directly, and from that infer y . However, to query each N -fold product Π_x one must query all N unitaries; and there are P such products. Hence, the overall query complexity is $Q = O(NP) \geq O(N^2)$ if one considers $P \geq N$ (as we did in our experimental demonstration), i.e. quadratically worse in N than with the quantum N -switch. A third possibility could be to directly estimate the signs of the commutators between the Π_x ’s, and from that infer y . A canonical tool for that is the well-known Hadamard test [36]. This allows one to estimate overlaps of the form $\langle \Psi | \Pi_x | \Psi \rangle_t$ or $\langle \Psi | \Pi_x^\dagger \Pi_{x'} \Pi_x | \Psi \rangle_t$ directly from queries to Π_x or Π_x and $\Pi_{x'}$, respectively, for any state $|\Psi\rangle_t$. As before, each query to Π_x accounts for N queries to the gates, and the overall query complexity is again $Q = O(NP) \geq O(N^2)$.

Finally, one can simulate S_N exactly with a circuit with fixed gate orders. For the usual case where all $P = N!$ permutations are considered, the optimal causally ordered circuit that synthesizes S_N in the blackbox scenario displays complexity $Q = \Omega(N^2)$ [13, 14, 17]. For the concrete case experimentally studied here, $P = N = 4$, the optimal causally ordered circuit that synthesizes S_4 requires 9 queries (see App. 2). In fact, this is the reason why we chose the particular permutation set $\{ABCD, BADC, CBDA, DACB\}$. Through a brute-force search, we found that, from all quartets of permutations, most of them require 7 queries or less with the simulation strategy presented in App. 2, some other 8 queries, and a few of them (including the one chosen here) require the maximum of 9 queries. Thus, the specific version of the quantum 4-switch implemented here provides a gap of

$9 - 4 = 5$ queries with respect to all causally ordered processes.

B. Experimental details

Single photon source.— The single-photon light source is composed of a semiconductor distributed feedback telecom laser ($\lambda = 1546$ nm) connected to an external fiber-pigtailed amplitude modulator (MZI). An FPGA unit (FPGA1) was used with the MZI to externally modulate the laser and generate optical pulses 5 ns wide. Optical attenuators (ATT) are used before MZI to create weak coherent states with a mean photon number per pulse of $\mu = 0.2$. In this case, 90% of the non-null pulses generated contain a single photon. Thus, our source is a good approximation to a non-deterministic single-photon source, which is commonly adopted in quantum communications [45]. FPGA1 also controls the active phase stabilization of the system and registration of single-photon counts during the measurement procedure (see below).

Indistinguishability of the multi-gate operations in different orders.— The four unitary operators U_i ($i = A, B, C, D$) were realized using birefringent liquid crystal retarders. An important aspect of the experiment is to guarantee the realization of the same unitary operation U_i , for all different orders considered. That is, the implementation of U_i must be independent of the illuminated core on the corresponding 4CF at the IN side of the oracle. To achieve this, the LCRs are placed in the Fourier plane of the objective lenses of the 4CF fiber launchers [see Fig. 4 (a)]. At the exit face of this fiber, the output single mode of each core is given by a gaussian function $g(\vec{r})$ centered at the core position \vec{r}_c . At the Fourier plane of the launcher lens, the spatial distribution of each core is given by the Fourier transform $\mathcal{F}[g(\vec{r} - \vec{r}_c)](\vec{s}) \propto \exp(ik\vec{s} \cdot \vec{r}_c/f)g(\vec{s})$. Therefore, irrespective of the illuminated core, all core modes overlap at the same central point with the intensity proportional to $|g(\vec{s})|^2$. This avoids spatial distinctions as in certain implementations for $N = 2$ gates [18, 19]. To guarantee this condition for our experiment, we used a CCD camera to record the intensity distributions at the Fourier plane (with the LCRs removed), as shown in Fig. 4 (b). The images, obtained with an intense laser, show the centering of the light distribution when a single core is connected. The resulting interference pattern when all cores are illuminated shows high-visibility, confirming spatial indistinguishability. This guarantees that the unitary operations U_i are indistinguishable when applied in different orders— a crucial requirement for a valid implementation of an N -switch [20].

Phase stabilization and Measurement procedure.— Phase (PHASE MOD) and intensity modulators (INT MOD) are used after the first 4CF-BS, on each arm of the interferometer (see Fig. 2 (a)), to set the relative phases between the four spatial modes to zero, and to adjust the amplitudes. The FPGA1 unit is used to implement a control system to actively compensate phase-drifts in the quantum 4-switch. The control is based on a perturb and observe power point tracking method [39, 46]. Basically, the phase drift compensation al-

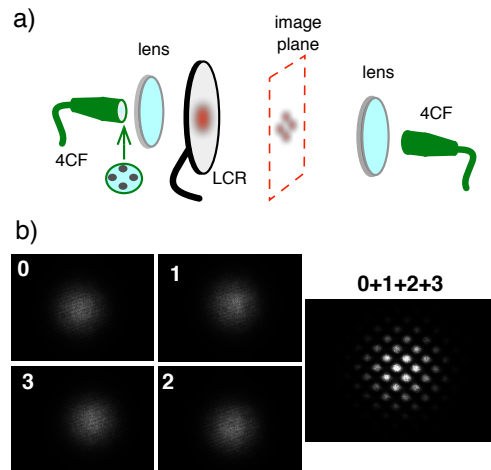


Figure 4. a) Illustration of the 4CF launchers and the liquid crystal retarders (LCR) implementing the unitaries U_i . The LCRs are placed at the Fourier plane of the output coupling lenses. b) Images recorded at the LCRs plane, of each core alone, as well as the output when all cores are connected, showing large spatial overlap between the cores modes. This guarantees that U_i 's are indistinguishable when applied in different orders.

gorithm will perturb the k th phase modulator to cancel any phase noise using a high-speed signal. The algorithm does this sequentially to each phase modulator and in each step it maximizes the number of photo-counts in the output detector “0” with the LCRs set to realize column $y = 0$ of one of the tables in Table 1. When the counts achieve a given threshold value for the success probability, the voltages applied to the phase modulators are maintained constant, and an ON signal is sent to FPGA2 to activate the LCRs by applying a constant voltage, realizing any one of the four columns of the respective table in Table 1, chosen by the user. After a 0.2 s deadtime to allow for the LCRs voltages to reach the desired value, a 0.1 s measurement stage is realized. After a single measurement window, an OFF signal is sent to return the LCRs to column 0. In this way, we can switch rapidly between columns 0-3 of the tables. The control system monitors the phase stabilization of the interferometer in real-time after every measurement.

We have used this phase stabilization routine in other work [39], and obtained visibilities over 99%. Here, our success probability is limited to about 95% due to slightly imperfect polarization rotations of the LCRs, as well as the difficulty in achieving proper alignment of the polarization state for the different LCR combinations in each path, which we observed in the initial alignment procedure using the polarimeter (see section IV).

ACKNOWLEDGEMENTS

We thank Barbara Amaral, Johanna Barra, Fabio Costa and Časlav Brukner for helpful insights. MMT and LA acknowledge financial support from the Brazilian agencies CNPq (PQ grant No. 311416/2015-2 and INCT-IQ), FAPERJ (PDR10

E-26/202.802/2016 and JCN E-26/202.701/2018), CAPES (PROCAD2013), and the Serrapilheira Institute (grant number Serra-1709-17173). This work was also supported by Fondo Nacional de Desarrollo Científico y Tecnológico (ANID) (3200779, 1190901, 1200266, 1200859) and ANID – Millennium Science Initiative Program – ICN17_012. JC was supported by ANID/REC/PAI77190088. AA was sup-

ported by the Swiss National Science Foundation (Starting Grant DIAQ and NCCR SwissMAP). MA has received funding from the European Union’s Horizon 2020 research and innovation programme under the Marie Skłodowska-Curie grant agreement No 801110 and the Austrian Federal Ministry of Education, Science and Research (BMBWF). It reflects only the author’s view, the EU Agency is not responsible for any use that may be made of the information it contains.

-
- [1] O. Oreshkov, F. Costa, and Č. Brukner, Quantum correlations with no causal order, *Nature Communications* **3**, 1092 (2012), arXiv:1105.4464.
- [2] M. Araújo, C. Branciard, F. Costa, A. Feix, C. Giarmatzi, and Č. Brukner, Witnessing causal nonseparability, *New Journal of Physics* **17**, 102001 (2015), arXiv:1506.03776.
- [3] O. Oreshkov and C. Giarmatzi, Causal and causally separable processes, *New Journal of Physics* **18**, 093020 (2016), arXiv:1506.05449.
- [4] L. Hardy, Probability Theories with Dynamic Causal Structure: A New Framework for Quantum Gravity, (2005), arXiv:0509120 [gr-qc].
- [5] L. Hardy, Towards quantum gravity: A framework for probabilistic theories with non-fixed causal structure, *Journal of Physics A: Mathematical and Theoretical* **40**, 3081 (2007), arXiv:0608043 [gr-qc].
- [6] L. Hardy, Quantum Gravity Computers: On the Theory of Computation with Indefinite Causal Structure, in *Quantum Reality, Relativistic Causality, and Closing the Epistemic Circle: Essays in Honour of Abner Shimony* (Springer Netherlands, Dordrecht, 2009) pp. 379–401, arXiv:0701019 [quant-ph].
- [7] G. Chiribella, G. M. D’Ariano, P. Perinotti, and B. Valiron, Quantum computations without definite causal structure, *Physical Review A* **88**, 022318 (2013), arXiv:0912.0195.
- [8] M. Araújo, P. A. Guérin, and Ä. Baumeler, Quantum computation with indefinite causal structures, *Physical Review A* **96**, 052315 (2017), arXiv:1706.09854.
- [9] M. Zych, F. Costa, I. Pikovski, and Č. Brukner, Bell’s theorem for temporal order, *Nature Communications* **10**, 3772 (2019), arXiv:1708.00248.
- [10] G. Chiribella, G. M. D’Ariano, and P. Perinotti, Quantum Circuit Architecture, *Physical Review Letters* **101**, 060401 (2008), arXiv:0712.1325.
- [11] G. Chiribella, G. M. D’Ariano, and P. Perinotti, Theoretical framework for quantum networks, *Physical Review A* **80**, 022339 (2009), arXiv:0904.4483.
- [12] G. Chiribella, Perfect discrimination of no-signalling channels via quantum superposition of causal structures, *Physical Review A* **86**, 040301(R) (2012), arXiv:1109.5154.
- [13] T. Colnaghi, G. M. D’Ariano, S. Facchini, and P. Perinotti, Quantum computation with programmable connections between gates, *Physics Letters A* **376**, 2940 (2012).
- [14] M. Araújo, F. Costa, and Č. Brukner, Computational Advantage from Quantum-Controlled Ordering of Gates, *Physical Review Letters* **113**, 250402 (2014), arXiv:1401.8127.
- [15] P. A. Guérin, A. Feix, M. Araújo, and Č. Brukner, Exponential Communication Complexity Advantage from Quantum Superposition of the Direction of Communication, *Physical Review Letters* **117**, 100502 (2016), arXiv:1605.07372.
- [16] K. Wei, N. Tischler, S.-r. Zhao, Y.-H. Li, J. M. Arrazola, Y. Liu, W. Zhang, H. Li, L. You, Z. Wang, Y.-a. Chen, B. C. Sanders, Q. Zhang, G. J. Pryde, F. Xu, and J.-W. Pan, Experimental Quantum Switching for Exponentially Superior Quantum Communication Complexity, *Physical Review Letters* **122**, 120504 (2019), arXiv:1810.10238.
- [17] S. Facchini and S. Perdrix, Quantum Circuits for the Unitary Permutation Problem, in *Theory and Applications of Models of Computation, Proceedings, Lecture Notes in Computer Science*, Vol. 9076, edited by R. Jain, S. Jain, and F. Stephan (Springer International Publishing, 2015) pp. 324–331.
- [18] L. M. Procopio, A. Moqanaki, M. Araújo, F. Costa, I. Alonso Calafell, E. G. Dowd, D. R. Hamel, L. A. Rozema, Č. Brukner, and P. Walther, Experimental superposition of orders of quantum gates, *Nature Communications* **6**, 7913 (2015), arXiv:1412.4006.
- [19] G. Rubino, L. A. Rozema, A. Feix, M. Araújo, J. M. Zener, L. M. Procopio, Č. Brukner, and P. Walther, Experimental verification of an indefinite causal order, *Science Advances* **3**, e1602589 (2017), arXiv:1608.01683.
- [20] K. Goswami, C. Giarmatzi, M. Kewming, F. Costa, C. Branciard, J. Romero, and A. G. White, Indefinite Causal Order in a Quantum Switch, *Physical Review Letters* **121**, 090503 (2018), arXiv:1803.04302.
- [21] Y. Guo, X.-M. Hu, Z.-B. Hou, H. Cao, J.-M. Cui, B.-H. Liu, Y.-F. Huang, C.-F. Li, G.-C. Guo, and G. Chiribella, Experimental Transmission of Quantum Information Using a Superposition of Causal Orders, *Physical Review Letters* **124**, 030502 (2020), arXiv:1811.07526.
- [22] K. Goswami, Y. Cao, G. A. Paz-Silva, J. Romero, and A. G. White, Communicating via ignorance (2018), arXiv:1807.07383.
- [23] D. Deutsch and R. Jozsa, Rapid solution of problems by quantum computation, *Proceedings of the Royal Society of London. Series A: Mathematical and Physical Sciences* **439**, 553 (1992).
- [24] D. R. Simon, On the Power of Quantum Computation, *SIAM Journal on Computing* **26**, 1474 (1997).
- [25] M. A. Nielsen and I. L. Chuang, *Quantum Computation and Quantum Information* (Cambridge University Press, Cambridge, 2010).
- [26] N. Friis, V. Dunjko, W. Dür, and H. J. Briegel, Implementing quantum control for unknown subroutines, *Physical Review A* **89**, 030303(R) (2014), arXiv:1401.8128.
- [27] O. Oreshkov, Time-delocalized quantum subsystems and operations: on the existence of processes with indefinite causal structure in quantum mechanics, *Quantum* **3**, 206 (2019), arXiv:1801.07594.
- [28] D. J. Richardson, J. M. Fini, and L. E. Nelson, Space-division multiplexing in optical fibres, *Nature Photonics* **7**, 354 (2013), arXiv:1303.3908.
- [29] G. Cañas, N. Vera, J. Cariñe, P. González, J. Cardenas, P. W. R. Connolly, A. Przysieszna, E. S. Gómez, M. Figueroa, G. Vallone, P. Villoresi, T. F. da Silva, G. B. Xavier, and G. Lima,

- High-dimensional decoy-state quantum key distribution over multicore telecommunication fibers, *Physical Review A* **96**, 22317 (2017), arXiv:1610.01682.
- [30] Y. Ding, D. Bacco, K. Dalgaard, X. Cai, X. Zhou, K. Rottwitt, and L. K. Oxenløwe, High-dimensional quantum key distribution based on multicore fiber using silicon photonic integrated circuits, *npj Quantum Information* **3**, 25 (2017), arXiv:1610.01812.
- [31] G. B. Xavier and G. Lima, Quantum information processing with space-division multiplexing optical fibres, *Communications Physics* **3**, 9 (2020), arXiv:1905.12644.
- [32] L. M. Procopio, F. Delgado, M. Enríquez, N. Belabas, and J. A. Levenson, Communication Enhancement through Quantum Coherent Control of N Channels in an Indefinite Causal-Order Scenario, *Entropy* **21**, 1012 (2019), arXiv:1902.01807.
- [33] L. M. Procopio, F. Delgado, M. Enríquez, N. Belabas, and J. A. Levenson, Sending classical information via three noisy channels in superposition of causal orders, *Physical Review A* **101**, 012346 (2020), arXiv:1910.11137.
- [34] M. Araújo, A. Feix, M. Navascués, and Č. Brukner, A purification postulate for quantum mechanics with indefinite causal order, *Quantum* **1**, 10 (2017), arXiv:1611.08535.
- [35] M. M. Taddei, R. V. Nery, and L. Aolita, Quantum superpositions of causal orders as an operational resource, *Physical Review Research* **1**, 033174 (2019), arXiv:1903.06180.
- [36] K. J. Horadam, *Hadamard Matrices and Their Applications* (Princeton University Press, Princeton, 2007).
- [37] A. Y. Kitaev, Quantum measurements and the Abelian Stabilizer Problem (1995), arXiv:9511026 [quant-ph].
- [38] E. A. Aguilar, M. Farkas, D. Martínez, M. Alvarado, J. Cariñe, G. B. Xavier, J. F. Barra, G. Cañas, M. Pawłowski, and G. Lima, Certifying an Irreducible 1024-Dimensional Photonic State Using Refined Dimension Witnesses, *Physical Review Letters* **120**, 230503 (2018), arXiv:1710.04601.
- [39] J. Cariñe, G. Cañas, P. Skrzypczyk, I. Šupić, N. Guerrero, T. Garcia, L. Pereira, M. A. S. Prosser, G. B. Xavier, A. Delgado, S. P. Walborn, D. Cavalcanti, and G. Lima, Multiport beamsplitters based on multi-core optical fibers for high-dimensional quantum information, (2020), arXiv:2001.11056.
- [40] K. Watanabe, T. Saito, K. Imamura, and M. Shiino, Development of fiber bundle type fan-out for multicore fiber, in *IEEE 17th Opto-Electronics and Communications Conference* (2012) pp. 5C1—2.
- [41] Y. Tottori, T. Kobayashi, and M. Watanabe, Low Loss Optical Connection Module for Seven-Core Multicore Fiber and Seven Single-Mode Fibers, *IEEE Photonics Technology Letters* **24**, 1926 (2012).
- [42] S. P. Walborn, M. O. Terra Cunha, S. Pádua, and C. H. Monken, Double-slit quantum eraser, *Physical Review A* **65**, 33818 (2002), arXiv:0106078 [quant-ph].
- [43] F. A. Torres-Ruiz, G. Lima, A. Delgado, S. Pádua, and C. Saavedra, Decoherence in a double-slit quantum eraser, *Physical Review A* **81**, 42104 (2010), arXiv:0911.0330.
- [44] C. Branciard, Witnesses of causal nonseparability: an introduction and a few case studies, *Scientific Reports* **6**, 26018 (2016), arXiv:1603.00043.
- [45] N. Gisin, G. Ribordy, W. Tittel, and H. Zbinden, Quantum cryptography, *Reviews of Modern Physics* **74**, 145 (2002), arXiv:quant-ph/0101098.
- [46] P. Bhatnagar and R. K. Nema, Maximum power point tracking control techniques: State-of-the-art in photovoltaic applications, *Renewable and Sustainable Energy Reviews* **23**, 224 (2013).
- [47] M. Araújo, A. Feix, F. Costa, and Č. Brukner, Quantum circuits cannot control unknown operations, *New Journal of Physics* **16**, 93026 (2014), arXiv:1309.7976.
- [48] J. Thompson, K. Modi, V. Vedral, and M. Gu, Quantum plug 'n' play: modular computation in the quantum regime, *New Journal of Physics* **20**, 013004 (2018), arXiv:1310.2927.
- [49] A. A. Abbott, J. Wechs, D. Horsman, M. Mhalla, and C. Branciard, Communication through coherent control of quantum channels, *Quantum* **4**, 333 (2020), arXiv:1810.09826.
- [50] G. Chiribella and H. Kristjánsson, Quantum Shannon theory with superpositions of trajectories, *Proceedings of the Royal Society A: Mathematical, Physical and Engineering Sciences* **475**, 20180903 (2019), arXiv:1812.05292.
- [51] H. Kristjánsson, G. Chiribella, S. Salek, D. Ebler, and M. Wilson, Resource theories of communication, *New Journal of Physics* **22**, 073014 (2020), arXiv:1910.08197.
- [52] P. Koutas and T. Hu, Shortest string containing all permutations, *Discrete Mathematics* **11**, 125 (1975).
- [53] M.-D. Choi, Completely positive linear maps on complex matrices, *Linear Algebra and its Applications* **10**, 285 (1975).
- [54] J. Wechs, H. Dourdent, A. A. Abbott, and C. Branciard, Quantum circuits with classical versus quantum control of causal orders, In preparation.
- [55] J. Wechs, A. A. Abbott, and C. Branciard, On the definition and characterisation of multipartite causal (non)separability, *New Journal of Physics* **21**, 013027 (2019), arXiv:1807.10557.
- [56] B. O'Donoghue, E. Chu, N. Parikh, and S. Boyd, Conic Optimization via Operator Splitting and Homogeneous Self-Dual Embedding, *Journal of Optimization Theory and Applications* **169**, 1042 (2016).
- [57] B. O'Donoghue, E. Chu, N. Parikh, and S. Boyd, SCS: Splitting conic solver, version 2.1.2 (2019).
- [58] D. Gross, J. Eisert, N. Schuch, and D. Perez-Garcia, Measurement-based quantum computation beyond the one-way model, *Physical Review A* **76**, 052315 (2007), arXiv:0706.3401.
- [59] Aidan Roy and A. J. Scott, "Unitary designs and codes," *Designs, Codes and Cryptography* **53**, 13–31 (2009), arXiv:0809.3813.

APPENDIX

1. Proof of Eq. (5).

First, note that (just like the Fourier transform) the Hadamard gate H_P maps $|0\rangle_c$ to the uniform superposition of all computational-basis states (under the assumption that the corresponding Hadamard matrix M_P only has +1 values along the first column):

$$H_P |0\rangle_c |\Psi\rangle_t = \frac{1}{\sqrt{P}} \sum_{x \in [P]} |x\rangle_c |\Psi\rangle_t. \quad (7)$$

Then, the quantum N -switch gate introduces the sign $m_{x,y}$ to each computational-basis state $|x\rangle_c$ in the superposition:

$$\begin{aligned} S_N H_P |0\rangle_c |\Psi\rangle_t &= \frac{1}{\sqrt{P}} \sum_{x \in [P]} |x\rangle_c \Pi_x |\Psi\rangle_t \\ &= \left(\frac{1}{\sqrt{P}} \sum_{x \in [P]} m_{x,y} |x\rangle_c \right) \Pi_0 |\Psi\rangle_t, \end{aligned} \quad (8)$$

where the second equality follows from Eq. (4). Now, by definition, the state within the brackets is $H_P |y\rangle_c$. Hence, applying H_P^{-1} to both sides of Eq. (8) yields Eq. (5). \square

2. Exact simulation of the quantum N -switch with a fixed-gate-order circuit

It is possible to simulate the quantum N -switch – i.e. produce the same superposition of unitaries $\{\Pi_x\}_{x \in [P]}$ as the quantum N -switch for whatever unitaries U_i are inserted at its open slots – with a causally ordered circuit at the cost of making more uses (queries) of each unitary. The basic idea behind such circuit is to apply the unitaries coherently controlled by a qudit. However, this is not a straightforward task with black-box unitaries [26, 47–51]. A workaround is to use ancillas and controlled swap gates that coherently control whether each target-system gate is effectively applied to the target system or to an ancilla. This can be done with a circuit such as in Fig. 5, which uses a P -dimensional control qudit and N d -dimensional ancilla systems (one for each gate U_i). Importantly, as the reader may verify, all N ancillas experience the same overall gate sequence for all input states of the control register, which guarantees that the ancillas disentangle from the target and control systems by the end of the circuit. For instance, for the circuit in Fig. 5, the final state of the ancillas is $U_A^2 |0\rangle_{\text{anc},A} U_B |0\rangle_{\text{anc},B} U_C |0\rangle_{\text{anc},C} U_D |0\rangle_{\text{anc},D}$.

With this circuit scheme, the problem of simulating the superposition of unitaries produced by a quantum N -switch reduces to finding a supersequence that includes all the desired permutations as subsequences; the query complexity of this scheme is then given by the length of the shortest such supersequence [17, 52]. In the experiment and Fig. 5, $ACBADACDB$ is the supersequence to the quartet of permutations $\{ABCD, BADC, CBDA, DACB\}$ (notice that the subsequences need not be contiguous). We have made an extensive numerical search of all quartets of permutations of A, B, C, D . There are $\binom{N-1}{P-1} = \binom{23}{3} = 1771$ unique quartets, where quartets that differ only by relabeling are disregarded (this amounts to, for instance, only considering quartets that include some fixed permutation, e.g. $ABCD$). Of those, most require a supersequence of length 8 or less (37 unique quartets require length 6; 946 require length 7; 779 require length 8) and only 9 require length 9. Since the higher the supersequence length, the higher the query complexity of the simulation by fixed-gate-order circuit, we chose one of the latter 9 quartets for our experiment (as well as Fig. 5). Notice that all 9 black boxes are queried once, irrespective of whether they are effectively used in the superposition or not, hence the

query complexity of this simulation of the quantum 4-switch is 9.

3. Fixed-gate circuit algorithms for the Hadamard promise problem exploiting side information about the gates

Let us revisit the adversarial scenario of a Verifier who controls the oracle and poses the Hadamard promise problem to a Prover. The Prover thus receives unknown (to them) unitaries and uses them to the best of their abilities to solve the problem and output the correct answer to the Verifier. As we showed, a Prover in possession of a quantum N -switch can solve the problem with 100% success rate using only a single query from each unitary. We now ask: can a Prover solve the problem with access only to fixed-gate-order circuits?

By performing the simulations in the previous section, they are also able to solve the Hadamard promise problem with 100% success rate. However, they must request additional queries of the oracle to the Verifier, a tell-tale sign to the latter that the quantum N -switch has not been realized.

We now explore the case of a Prover with side information on the unitaries from the oracle. More specifically, let us suppose they know the table of unitaries that the Verifier uses (Table 1a or 1b), but not which column is selected in each run. This information aids the Prover, who may no longer need to produce the superposition of unitaries from the previous section.

If Table 1a is used, the Prover’s strategy is relatively simple. By inputting a $|+\rangle := (|0\rangle + |1\rangle)/\sqrt{2}$ state to black box U_A , the output state will be either $|+\rangle$, if $U_A = \mathbb{1}$, or $|-\rangle := (|0\rangle - |1\rangle)/\sqrt{2}$, if $U_A = Z$. With a measurement of the output in the X basis, they can identify U_A (we call this an X -basis test on U_A). Doing the same procedure on U_C , they identify this unitary as well and discover the column y of Table 1a being used. Since only 1 query or less of each unitary is needed, the Prover can in fact deceive the Verifier in this case.

If instead Table 1b is used, the Prover requires a slightly more complex fixed-gate-order circuit to deceive the Verifier. It begins with an X -basis test on applied to U_C , which reveals the content of that black box. In turn, U_D is revealed with an analogous Z -basis test, with input state $|0\rangle$ and measurement of output in the Z basis. If one of these two black boxes is revealed to be a Pauli operator (Z or X , resp.), then that run of the promise problem has been solved ($y = 1$ or 3 , resp). However, if both $U_C = \mathbb{1}$ and $U_D = \mathbb{1}$, both $y = 0$ and $y = 2$ are possible, and the black boxes U_A, U_B need to be used. Since the quantum N -switch finds the correct value of y with probability one, so is the goal of the Prover here. However, the two possible unitaries for U_A ($\frac{Z+X}{\sqrt{2}}, Z$) are not orthogonal, i.e. not perfectly distinguishable, and the same happens with U_B . No independent use of U_A and U_B can tell the columns apart with certainty. There is a viable strategy, though, using U_A and U_B in sequence. Notice indeed that $U_B U_A = \mathbb{1}$ for column 0 and $U_B U_A = -iY$ for column 2. A Z - or X -basis test applied to the sequence of the two unitaries U_A and U_B can distinguish these two possibilities, again solving the problem with certainty.

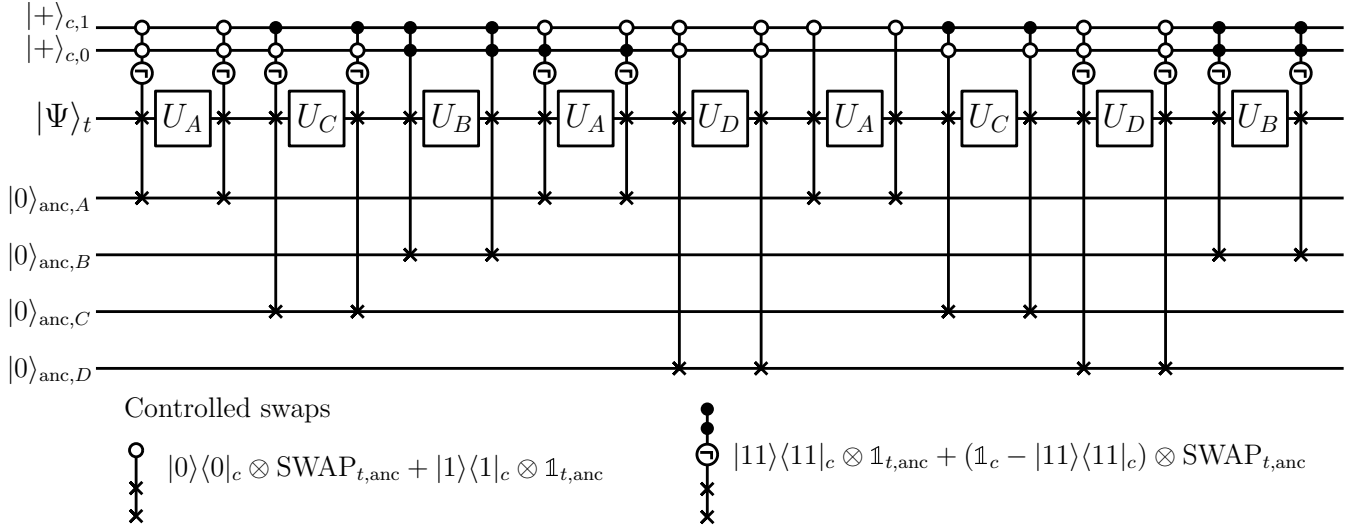


Figure 5. Fixed-gate-order circuit that simulates the quantum 4-switch that was realized experimentally, i.e. with quantum control of the four gate sequences $\Pi_0 = U_D U_C U_B U_A$, $\Pi_1 = U_C U_D U_A U_B$, $\Pi_2 = U_A U_D U_B U_C$, and $\Pi_3 = U_B U_C U_A U_D$. Before and after each unitary U_i , a pair of controlled swap gates controls whether U_i is applied to the target system or to an ancilla; the control qudit has dimension $P = 4$, here represented as two qubits (with $x = 0, 1, 2$ and 3 encoded as $00, 01, 10$ and 11 , resp.). Black dots indicate an operation conditioned on the $|1\rangle_c$ state, white dots, conditioned on the $|0\rangle_c$ state. Conditioning on negation of certain states is also needed, as exemplified in the legend below the circuit.

If the Prover does not know whether the Verifier uses Table 1a or 1b, the former needs to first identify which table is used. This table identification can be done with a Z -basis test on U_D , which reveals whether $U_D = X$ or $U_D = \mathbb{1}$. The strategy for Table 1a is applied in the former case, that for Table 1b in the latter (notice that column $y = 3$ is the same for both tables).

4. Causal witnesses for the 4-switch process

In order to certify, via the Hadamard promise problem, that a given process exhibits some quantum control of gate orders (QCGO), one may look for the maximal probability of success $p_{\text{succ}}^{\text{CCGO}}$ that processes with *classical* control of gate orders (CCGO) can reach: If this upper bound is strictly smaller than 1, it becomes possible to experimentally obtain a probability of success $p_{\text{succ}} > p_{\text{succ}}^{\text{CCGO}}$ and thus prove that these results cannot be explained by CCGO.

For a fixed choice of gate permutations and of Hadamard matrix under consideration, the “causal bound” $p_{\text{succ}}^{\text{CCGO}}$ still depends on the specific choice of possible sets \mathbf{U} , and of the prior distribution with which each set is chosen in each experimental run. Considering different possible sets \mathbf{U}_k , each satisfying the promise of Eq. (4) for some value $y = y_k$ and chosen with probability q_k , the probability of success (i.e., of obtaining the correct value $y = y_k$) of the Hadamard promise problem is obtained as

$$p_{\text{succ}} = \sum_k q_k \text{Prob}(y = y_k | \mathbf{U} = \mathbf{U}_k). \quad (9)$$

To compute the above probabilities, and to obtain the causal

bound $p_{\text{succ}}^{\text{CCGO}}$, we use the so-called “process matrix framework” [1]. In this framework the process under consideration (i.e., in our case, the circuit that connects the 4 unitaries and the final measurement) is described by the “process matrix” W , acting on the tensor product of all input and output Hilbert spaces of the 4 unitaries and of the final measurement. When the 4 qubit unitaries from some quartet $\mathbf{U}_k = \{U_A^{(k)}, U_B^{(k)}, U_C^{(k)}, U_D^{(k)}\}$ are applied, the probability $\text{Prob}(y = y_k | \mathbf{U} = \mathbf{U}_k)$ that the final measurement in the computational basis $\{|y\rangle_c\}_{y \in [4]}$ of \mathbb{H}_c gives the outcome y_k for an arbitrary process matrix W is obtained as

$$\text{Prob}(y = y_k | \mathbf{U} = \mathbf{U}_k) = \text{Tr} [(|\mathbf{U}_k\rangle\rangle\langle\langle \mathbf{U}_k|^T \otimes |y_k\rangle\langle y_k|_c) W] \quad (10)$$

with

$$|\mathbf{U}_k\rangle\rangle := |U_A^{(k)}\rangle\rangle |U_B^{(k)}\rangle\rangle |U_C^{(k)}\rangle\rangle |U_D^{(k)}\rangle\rangle. \quad (11)$$

Here, T denotes the transposition in the computational basis $\{|0\rangle, |1\rangle\}$ of \mathbb{H}_t and $|\mathbf{U}_i^{(k)}\rangle\rangle \in \mathbb{H}_t \otimes \mathbb{H}_t$ is the Choi vector representation [53] of the i th unitary $U_i^{(k)}$, for $i = A, B, C$ or D , technically defined as $|\mathbf{U}_i^{(k)}\rangle\rangle := \mathbb{1} \otimes U_i^{(k)} |\mathbb{1}\rangle$, with $|\mathbb{1}\rangle := |0\rangle|0\rangle + |1\rangle|1\rangle$. According to Eq. (9), the success probability is then obtained as

$$p_{\text{succ}} = \text{Tr} [G W] \quad \text{with} \quad G = \sum_k q_k |\mathbf{U}_k\rangle\rangle\langle\langle \mathbf{U}_k|^T \otimes |y_k\rangle\langle y_k|_c. \quad (12)$$

The process matrix describing the ideal 4-switch process of

Fig. 1 (b) is given by [2, 3] $W_4 = |w_4\rangle\langle w_4|$, where

$$\begin{aligned} |w_4\rangle &= |0\rangle^{c_p} |\mathbb{1}\rangle^{t_p A_I} |\mathbb{1}\rangle^{A_O B_I} |\mathbb{1}\rangle^{B_O C_I} |\mathbb{1}\rangle^{C_O D_I} |\mathbb{1}\rangle^{D_O t_f} |0\rangle^{c_f} \\ &+ |1\rangle^{c_p} |\mathbb{1}\rangle^{t_p B_I} |\mathbb{1}\rangle^{B_O A_I} |\mathbb{1}\rangle^{A_O D_I} |\mathbb{1}\rangle^{D_O C_I} |\mathbb{1}\rangle^{C_O t_f} |1\rangle^{c_f} \\ &+ |2\rangle^{c_p} |\mathbb{1}\rangle^{t_p C_I} |\mathbb{1}\rangle^{C_O B_I} |\mathbb{1}\rangle^{B_O D_I} |\mathbb{1}\rangle^{D_O A_I} |\mathbb{1}\rangle^{A_O t_f} |2\rangle^{c_f} \\ &+ |3\rangle^{c_p} |\mathbb{1}\rangle^{t_p D_I} |\mathbb{1}\rangle^{D_O A_I} |\mathbb{1}\rangle^{A_O C_I} |\mathbb{1}\rangle^{C_O B_I} |\mathbb{1}\rangle^{B_O t_f} |3\rangle^{c_f} \end{aligned} \quad (13)$$

and the superscripts indicate the Hilbert spaces in which the various states are defined: c_p, c_f refer to the past and the future of the control system, t_p, t_f refer to the past and the future of the target system, A_I and A_O refer to the input and output spaces of operation U_A , and similarly for the other parties. Notice that, for the sake of clarity, Fig. 1a) uses a simplified notation based on the necessary isomorphism between t_p, t_f, A_I, A_O , and the other parties' inputs and outputs (as well as between c_p and c_f).

In Algorithm 1 we input the initial control state $H_P |0\rangle$ into c_p , the initial target state $|\Psi\rangle$ into t_p , and apply H_P^{-1} to the resulting state of the control system in c_f . These fixed steps can be incorporated into the process-matrix description. The resulting matrix that describes our effective process is then $W'_4 = \text{Tr}_{t_f} |w'_4\rangle\langle w'_4|$ with

$$\begin{aligned} |w'_4\rangle &= \frac{1}{2} \left[|\Psi\rangle^{A_I} |\mathbb{1}\rangle^{A_O B_I} |\mathbb{1}\rangle^{B_O C_I} |\mathbb{1}\rangle^{C_O D_I} |\mathbb{1}\rangle^{D_O t_f} H_P^{-1} |0\rangle_c \right. \\ &+ |\Psi\rangle^{B_I} |\mathbb{1}\rangle^{B_O A_I} |\mathbb{1}\rangle^{A_O D_I} |\mathbb{1}\rangle^{D_O C_I} |\mathbb{1}\rangle^{C_O t_f} H_P^{-1} |1\rangle_c \\ &+ |\Psi\rangle^{C_I} |\mathbb{1}\rangle^{C_O B_I} |\mathbb{1}\rangle^{B_O D_I} |\mathbb{1}\rangle^{D_O A_I} |\mathbb{1}\rangle^{A_O t_f} H_P^{-1} |2\rangle_c \\ &\left. + |\Psi\rangle^{D_I} |\mathbb{1}\rangle^{D_O A_I} |\mathbb{1}\rangle^{A_O C_I} |\mathbb{1}\rangle^{C_O B_I} |\mathbb{1}\rangle^{B_O t_f} H_P^{-1} |3\rangle_c \right]. \end{aligned} \quad (14)$$

Using this process matrix we can verify that for any set $U_k = \{U_A^{(k)}, U_B^{(k)}, U_C^{(k)}, U_D^{(k)}\}$ satisfying the promise (4) for some $y = y_k$, one has $\text{Tr} [(|U_k\rangle\langle U_k|^T \otimes |y_k\rangle\langle y_k|_c) W'_4] = 1$, so that the success probability of Algorithm 1, using the 4-switch, is indeed unity.

Processes that display CCGO, on the other hand, are described by process matrices from a particular subset of all possible matrices, with some specific structure. In Ref. 54, it is indeed shown that (in our scenario, with 4 operations and a final measurement) CCGO process matrices W must have a decomposition of the form

$$W = \sum_{(i,j,k,l)} W_{(i,j,k,l),c} \quad (15)$$

in terms of positive semidefinite matrices (not necessarily valid process matrices) $W_{(i,j,k,l),c}$, for all $4! = 24$ permutations (i, j, k, l) of $\{A, B, C, D\}$ (hence with $i \neq j \neq k \neq l$). These must furthermore be such that the ‘‘reduced’’ matrices $W_{(i,j,k,l)} := \text{Tr}_c W_{(i,j,k,l),c}$ (where c refers to the space of the final measurement), $W_{(i,j,k)} := \text{Tr}_l W_{(i,j,k,l)}$ (where Tr_l corresponds to the partial trace over the input and output spaces of the operation U_l), $W_{(i,j)} := \sum_k \text{Tr}_k W_{(i,j,k)}$ and

$W_{(i)} := \sum_j \text{Tr}_j W_{(i,j)}$ are of the form

$$\begin{aligned} W_{(i,j,k,l)} &= \widetilde{W}_{(i,j,k,l)} \otimes \mathbb{1}^{l_o}, & W_{(i,j,k)} &= \widetilde{W}_{(i,j,k)} \otimes \mathbb{1}^{k_o}, \\ W_{(i,j)} &= \widetilde{W}_{(i,j)} \otimes \mathbb{1}^{j_o}, & W_{(i)} &= \widetilde{W}_{(i)} \otimes \mathbb{1}^{i_o} \end{aligned} \quad (16)$$

for some matrices $\widetilde{W}_{(\dots)}$ in the appropriate spaces. Here $\mathbb{1}^{l_o}$ denotes the identity operator on the output space of the operation U_l , and similarly for $\mathbb{1}^{k_o}, \mathbb{1}^{j_o}$ and $\mathbb{1}^{i_o}$.

To obtain the causal bound $p_{\text{succ}}^{\text{CCGO}}$ for all CCGO processes – for a fixed choice of sets U_k and weights q_k , hence a fixed operator G as defined in Eq. (12) – one can then optimize the value of $p_{\text{succ}} = \text{Tr}[GW]$ for all W in the class described by Eqs. (15)–(16) above (which describes a closed convex cone, which we denote $\mathcal{W}^{\text{CCGO}}$) and with the additional normalisation condition [1, 3, 55] that $\text{Tr} W = 2^4$:

$$\begin{aligned} p_{\text{succ}}^{\text{CCGO}} &= \max_W \text{Tr} [GW] \\ \text{s.t. } &W \in \mathcal{W}^{\text{CCGO}}, \text{Tr} W = 2^4. \end{aligned} \quad (17)$$

As it turns out, this optimisation is a semidefinite programming (SDP) problem, which can in principle be solved faithfully [2, 44, 55].

Another possible, ‘‘dual’’ approach – now just for a fixed choice of possible sets U_k – is to optimize the causal witness rather than the process matrix. Fixing the witness to be of the form of G in Eq. (12), this allows us to optimize the weights q_k for each U_k : indeed the optimisation problem can be written here (see Appendix H in Ref. 2) as

$$\begin{aligned} p_{\text{succ}}^{\text{CCGO}} &= \min_{p, \{q_k\}_k} p \\ \text{s.t. } &p \mathbb{1}/2^4 - G \in \mathcal{S}^{\text{CCGO}}, \\ &G = \sum_k q_k |U_k\rangle\langle U_k|^T \otimes |y_k\rangle\langle y_k|_c, \\ &q_k \geq 0, \sum_k q_k = 1, \end{aligned} \quad (18)$$

where

$$\mathcal{S}^{\text{CCGO}} := (\mathcal{W}^{\text{CCGO}})^* := \{S \mid \forall W \in \mathcal{W}^{\text{CCGO}}, \text{Tr}[SW] \geq 0\} \quad (19)$$

is the convex cone dual to $\mathcal{W}^{\text{CCGO}}$, which can, like the latter, be described in terms of SDP constraints [2, 44, 55].

Let us note here that the above characterisation of $\mathcal{W}^{\text{CCGO}}$ (via the decomposition of Eq. (15), with the matrices $W_{(\dots)}$ satisfying the constraints of Eq. (16)) was shown [55] to be a sufficient condition for the process matrix to be ‘‘causally separable’’ [1, 3, 55]. It remains an open question, whether the class of causally separable processes is strictly larger than that of CCGO, or not. We nevertheless conjecture that the ‘‘causal bounds’’ $p_{\text{succ}}^{\text{CCGO}}$ we obtain here hold for all causally separable processes.

a. Causal witnesses with finitely many settings

As is clear from the discussion in App. 3, if one only uses the sets from Tables 1a and 1b, then one can only get a trivial

causal bound $p_{\text{succ}}^{\text{CCGO}} = 1$. In order to get a nontrivial bound, one needs to consider some other possible sets of unitaries.

To this end, we considered unitaries taken from the set

$$\mathcal{G} = \{\mathbb{1}, Z, X, Y, \frac{Z+X}{\sqrt{2}}, \frac{Z+Y}{\sqrt{2}}, \frac{X+Y}{\sqrt{2}}, \frac{\mathbb{1}+iZ}{\sqrt{2}}, \frac{\mathbb{1}+iX}{\sqrt{2}}, \frac{\mathbb{1}+iY}{\sqrt{2}}\} \quad (20)$$

(which have the nice property that their Choi matrices $|U\rangle\rangle\langle\langle U|$ span the full 10-dimensional space of all possible Choi matrices for qubit unitaries), and looked for which sets $U = \{U_A, U_B, U_C, U_D\}$ with $U_i \in \mathcal{G}$ satisfy the promise of Eq. (4). We found 460 different such sets: 316 satisfying the promise for $y = 0$, 60 for $y = 1$, 42 for $y = 2$ and again 42 for $y = 3$.

The SDP problem of Eq. (18) is large – indeed, G is a $2^{10} \times 2^{10}$ matrix and the characterisation of $\mathcal{S}^{\text{CCGO}}$ imposes many constraints – making it at the limits of tractability. To simplify the problem further, we exploit an approach based on “quantum superinstruments” introduced in Ref. [54]. To this end, we first note that Eq. (17) can be simplified by rewriting Eq. (12) in the form

$$\begin{aligned} p_{\text{succ}} &= \sum_y \text{Tr} [G^{[y]} W^{[y]}] \\ \text{with } G^{[y]} &= \sum_k \delta_{y,y_k} q_k |U_k\rangle\rangle\langle\langle U_k|_c^T \\ \text{and } W^{[y]} &= \text{Tr}_c[(\mathbb{1} \otimes |y\rangle\langle y|_c)W], \end{aligned} \quad (21)$$

(where δ_{y,y_k} is the Kronecker delta). Here, one now only needs to optimize over the four smaller $2^8 \times 2^8$ matrices $W^{[y]}$. The fact that the $W^{[y]}$'s must be obtained from some CCGO process as in the last line of Eq. (21) above implies similar SDP constraints as Eqs. (15)–(16) on the $W^{[y]}$'s directly [54]; more formally, one has $\{W^{[y]}\}_y \in \overline{\mathcal{W}}^{\text{CCGO}}$ where $\overline{\mathcal{W}}^{\text{CCGO}}$ is again a closed convex cone. The dual approach (18) can then also be rewritten in the simpler form

$$\begin{aligned} p_{\text{succ}}^{\text{CCGO}} &= \min_{p, \{q_k\}_k} p \\ \text{s.t. } &\{p \mathbb{1}/2^4 - G^{[y]}\}_y \in \overline{\mathcal{S}}^{\text{CCGO}}, \\ &G^{[y]} = \sum_k \delta_{y,y_k} q_k |U_k\rangle\rangle\langle\langle U_k|_c^T, \\ &q_k \geq 0, \sum_k q_k = 1, \end{aligned} \quad (22)$$

where the dual cone

$$\begin{aligned} \overline{\mathcal{S}}^{\text{CCGO}} &:= (\overline{\mathcal{W}}^{\text{CCGO}})^* \\ &:= \{\{S^{[y]}\}_y \mid \forall \{W^{[y]}\}_y \in \overline{\mathcal{W}}^{\text{CCGO}}, \\ &\quad \sum_y \text{Tr}[S^{[y]} W^{[y]}] \geq 0\} \end{aligned} \quad (23)$$

can again be described by SDP constraints [54].

We were able to solve the simpler SDP problem of Eq. (22) using the 460 sets of unitaries from \mathcal{G} with the solver SCS [56, 57], obtaining a bound of $p_{\text{succ}}^{\text{CCGO}} \approx 0.92$. We then progressively set to zero the smallest weights and solved the SDP again, eventually reaching 60 nonzero weights with no change in $p_{\text{succ}}^{\text{CCGO}}$ within numerical precision (36 corresponding to sets satisfying the promise for $y = 0$, 12 for $y = 1$, and 6 each for $y = 2$ and $y = 3$).

b. Causal witnesses with random rotations

The causal strategies described in App. 3 exploit knowledge of the basis that the unknown unitaries are defined in. A possibility to obtain better bounds on $p_{\text{succ}}^{\text{CCGO}}$ is therefore to allow the Verifier to provide the unitaries in an unknown basis. Given a set $U = \{U_A, U_B, U_C, U_D\}$, this corresponds formally to providing the operations $U^{(V)} = \{VU_A V^\dagger, VU_B V^\dagger, VU_C V^\dagger, VU_D V^\dagger\}$ for some unknown unitary V . Note that if U obeys the promise of Eq. (4) then so does $U^{(V)}$.

To construct better causal witnesses from this approach, we start as before with a fixed choice of sets U_k and then, in addition to choosing U_k with prior probability q_k , we randomly choose an unknown unitary V to be applied according to the Haar measure. Eq. (12) then becomes

$$\begin{aligned} p_{\text{succ}} &= \text{Tr} [G W] \\ \text{with } G &= \sum_k q_k \int d\mu(V) |U_k^{(V)}\rangle\rangle\langle\langle U_k^{(V)}|_c^T \otimes |y_k\rangle\langle y_k|_c, \end{aligned} \quad (24)$$

where $\mu(V)$ is the normalized Haar measure over $\text{SU}(2)$. The SDP problems (17), (18) and (21) can then be solved in the same way as described above.

We again consider the 460 sets of unitaries U with each $U_i \in \mathcal{G}$ as in the previous section. The integration over the Haar measure can be performed analytically by taking an explicit parameterisation of $\text{SU}(2)$ unitaries. However, since the $|U_k^{(V)}\rangle\rangle\langle\langle U_k^{(V)}|_c^T$ are $2^8 \times 2^8$ matrices, this procedure is nevertheless slow, even with automated symbolic integration using, e.g., Mathematica. To simplify matters, we exploit that fact that the Haar measure is unitary invariant (i.e., $d(V) = d(UV) = d(VU)$ for any unitary U), so sets U and U' that are equivalent up to a change of basis give $\int d\mu(V) |U^{(V)}\rangle\rangle\langle\langle U^{(V)}|_c = \int d\mu(V) |U'^{(V)}\rangle\rangle\langle\langle U'^{(V)}|_c$. We thereby find that there are 98 sets U which are inequivalent in this way and which satisfy one of the properties y_k .

Considering witnesses constructed from these sets, we solved the dual SDP problem given in Eq. (22). For CCGO processes, we find the bound $p_{\text{succ}}^{\text{CCGO}} \approx 0.84$. Interestingly, we find that the same bound can be reached by considering the Haar randomisation only over witnesses using sets U containing only Pauli matrices, rather than from the full set \mathcal{G} . Indeed, this bound can be obtained by randomising over the 30 sets U given in Table 2 that were found to have non-zero weights in the optimal witness we obtained.

c. Derandomization

In order not to require the assumption that the Prover does not know in which basis the Verifier provided each set U , one could derandomize the approach above by using a weighted quantum t -design [58]. This is a finite set of unitaries X together with weights w such that the average of any operator over them is equal to its average over the Haar measure up to

y	0	0	0	0	0	0	0	0	0	0	0	0	0	0	1	1	1	1	1	1	2	2	2	2	3	3	3	3	
U_A	$\mathbb{1}$	$\mathbb{1}$	$\mathbb{1}$	Z	$\mathbb{1}$	$\mathbb{1}$	Z	$\mathbb{1}$	Z	Z	$\mathbb{1}$	Z	Z	Z	Z	$\mathbb{1}$	Z	Z	Z	Z	$\mathbb{1}$	Z	Z	Z	$\mathbb{1}$	Z	Z	Z	
U_B	$\mathbb{1}$	$\mathbb{1}$	Z	$\mathbb{1}$	$\mathbb{1}$	Z	$\mathbb{1}$	Z	$\mathbb{1}$	Z	Z	$\mathbb{1}$	Z	Z	X	Z	$\mathbb{1}$	Z	X	X	X	Z	$\mathbb{1}$	X	Z	$\mathbb{1}$	X	X	X
U_C	$\mathbb{1}$	Z	$\mathbb{1}$	$\mathbb{1}$	Z	$\mathbb{1}$	$\mathbb{1}$	Z	Z	$\mathbb{1}$	Z	Z	$\mathbb{1}$	Z	X	X	$\mathbb{1}$	X	Z	X	Y	X	Z	$\mathbb{1}$	X	Z	$\mathbb{1}$	Z	Y
U_D	Z	$\mathbb{1}$	$\mathbb{1}$	$\mathbb{1}$	Z	Z	$\mathbb{1}$	$\mathbb{1}$	$\mathbb{1}$	Z	Z	Z	$\mathbb{1}$	Z	$\mathbb{1}$	X	X	X	Y	Z	Z	X	$\mathbb{1}$	Y	X	X	$\mathbb{1}$	Y	

Table 2. Table of 30 sets $U = \{U_A, U_B, U_C, U_D\}$ involving the identity $\mathbb{1}$ and the orthogonal Pauli operators X, Y, Z only, satisfying the promise of Eq. (4) (for some value of y , indicated in the first row), for the gate permutations $\Sigma = \{ABCD, BADC, CBDA, DACB\}$ and the Hadamard matrix of Eq. (6).

order t . Since $|U_k^{(V)}\rangle\rangle$ is an 8th order expression on V , an 8-design allows us to reproduce exactly the witness with bound $p_{\text{succ}}^{\text{CCGO}} \approx 0.84$ with a finite, fixed set of unitaries. Unfortunately, t -designs are rather large. It can be shown that the smallest size $|X|$ of a weighted 8-design for unitaries of dimension 2 is bounded by $165 \leq |X| \leq 968$, so the resulting witness would have at least 4950 settings, and therefore be of little relevance for experiments [59].

In order to obtain smaller witnesses, we instead sampled 5 random qubit unitaries from the Haar measure, and conjugated all 30 columns of Table 2 with these fixed unitaries,

obtaining a witness using 150 settings.

Solving the SDP in Eq. (17) with the solver SCS, fixing the prior probability of choosing each set $U_k^{(V)}$ to be $q_k/5$, where q_k is the optimal weight obtained for the full randomization of U_k in the previous section, we obtained $p_{\text{succ}}^{\text{CCGO}} \approx 0.96$. By further optimising over all 150 weights using the dual SDP, we found this could be improved to $p_{\text{succ}}^{\text{CCGO}} \approx 0.93$.

By using more than 5 random unitaries this bound can be lowered further. For example, with 10 random unitaries we were able to obtain $p_{\text{succ}}^{\text{CCGO}} \approx 0.89$ (when optimizing over all 300 weights).